Supplement of Hydrol. Earth Syst. Sci., 25, 2239–2259, 2021
https://doi.org/10.5194/hess-25-2239-2021-supplement

Hydrology and Earth System Sciences
Open Access
EGU

Supplement of

Quantifying the effects of land use and model scale on water partitioning and water ages using tracer-aided ecohydrological models

Aaron Smith et al.

Correspondence to: Aaron Smith (smith@igb-berlin.de)

Supplementary Material 1: Conceptual EcH$_2$O-iso energy and water balance

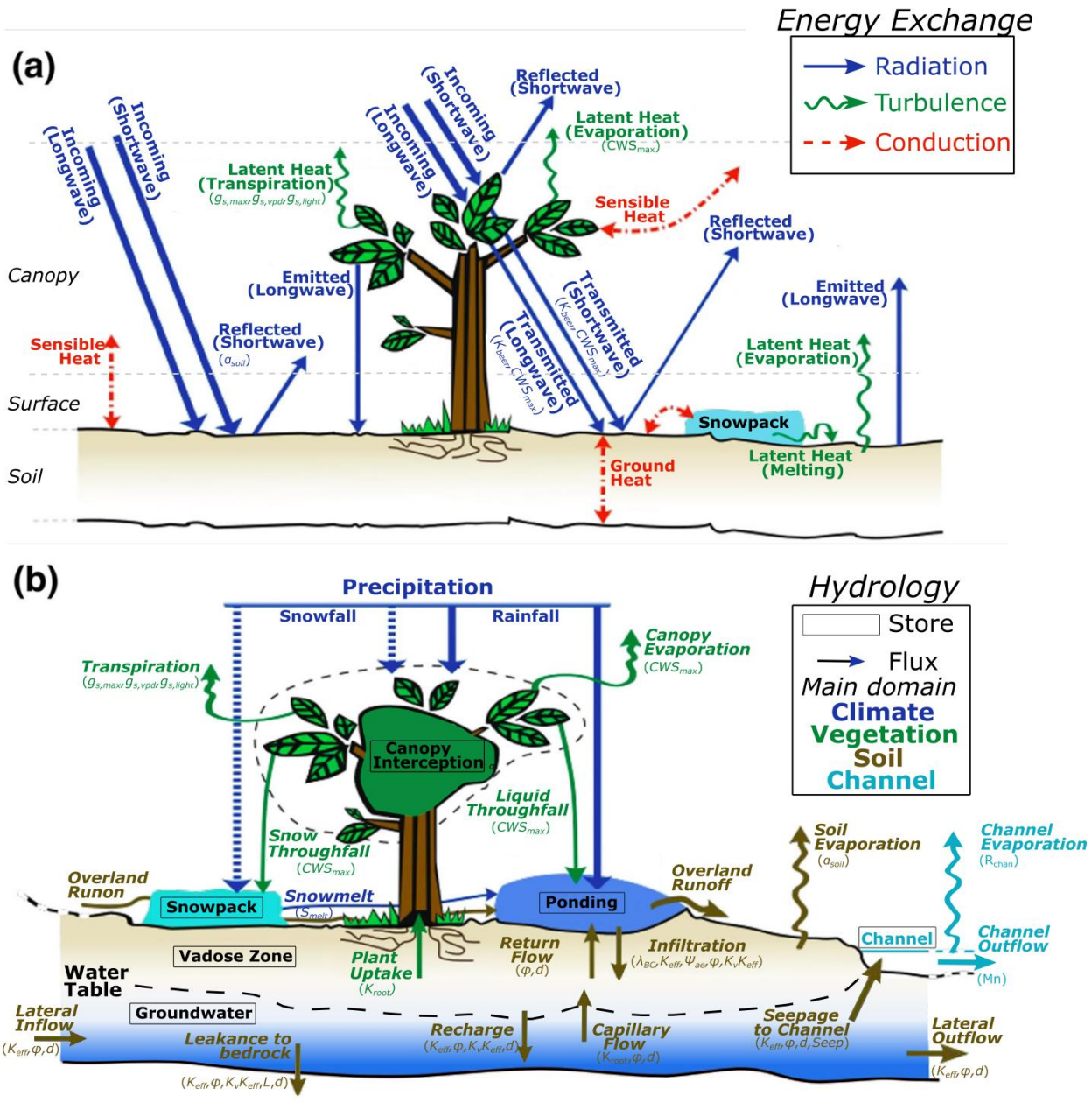

Figure S1: Conceptual framework of the energy and water balance storages and fluxes in the EcH2O (-iso) model. Parentheses below fluxes indicate parameters directly controlling each flux (adapted from Douinot et al. (2019)).

5

Supplementary Material 2: Multicriteria calibration, parameterisation, and validation

Due to the use of eCDFs, the overall efficiency ranges between 0 and 1, where a value of 1 indicates that all output from a given simulation is the best-observed model efficiency from all parameter sets. A value of 1 does not indicate that there is a perfect fit (e.g. may have Nash-Sutcliffe efficiency of 0.7 for discharge). Since trade-offs generally occur within multicriteria calibration (e.g. Boyle et al. (2000)), a value of 1 is not expected from any calibration. The values of overall efficiency indicate the threshold value, for example, 0.95 indicates the overall parameter sets were in the top 5% for all model output.

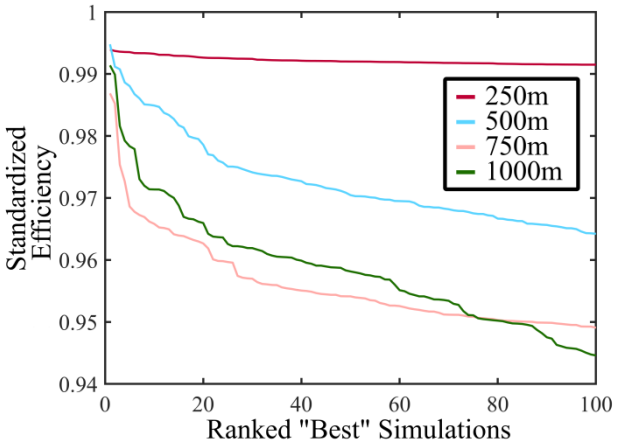

Figure S2: The standardized weighted multicriteria efficiency of each model scale, standardized against the best simulations of the given scale (100,000 simulations) and shown for the 100 "best" simulations.

Simulations in the finer resolution (250 and 500 m) show higher overall efficiency sustained for the 100 best simulations (Fig. S2). There is a very limited decrease in model performance for 250m in the 100 best simulations compared to the other resolutions which had a much more rapid decrease in overall model performance from the best to 100th best parameter set. There was a limited difference in the 750 and 1000m model resolutions for the rate of decrease in model performance (Fig. S2).

The overall best model performance is dependent on the best possible model efficiency of output for each resolution. Changing the model resolution independently changes the model efficiency (Table S1). In general, discharge, isotopes (stream, soil, and groundwater) have better possible model efficiency at finer resolutions, as indicated with the "Best Fit" (Table S1). Latent heat and evapotranspiration, calibrated against remote sensing data (MODIS), showed higher possible efficiency with coarser resolutions. Soil moisture simulations were inconsistent for both re-analysis data (ERA5) and field measurements, and were more dependent on the site (e.g. Forest A was better at coarser resolutions, Table S1).

Table S1: Best efficiency criteria for each model scale under single criteria calibration (i.e. best possible value for an output).

		250m	500m	750m	1000m	Best Fit
Discharge	**Demnitz Mill**	0.820	0.806	0.760	0.809	250m
	Demnitz	0.702	0.744	0.660	0.643	500m
Isotopes	**Peat North**	0.011	0.010	0.010	0.010	500m
	Peat South	0.014	0.016	0.020	0.018	250m
	Bruchmill	0.018	0.020	0.020	0.024	250m
	Demnitz Mill	0.023	0.024	0.023	0.025	750m
ET	**Conifers**	0.699	0.718	0.723	0.737	1000m
	Croplands	0.745	0.687	0.707	0.726	250m
	Forest A	0.744	0.663	0.756	0.766	1000m
Transpiration	**Forest A**	0.777	0.875	0.792	0.878	250m
Latent Heat	**Conifers**	0.705	0.732	0.727	0.734	1000m
	Croplands	0.583	0.548	0.555	0.641	1000m
	Forest A	0.624	0.568	0.681	0.668	750m
Soil Moisture (ERA 5)	**Alt Madlitz**	0.720	0.627	0.657	0.650	250m
	Forest A	0.696	0.663	0.713	0.732	1000m
Soil Moisture (Measured)	**Alt Madlitz**	0.729	0.663	0.661	0.660	250m
	Forest A	0.873	0.828	0.882	0.880	750m
Soil Isotopes	**Forest A**	0.066	0.073	0.068	0.082	250m
Groundwater Isotopes	**GW 4**	0.006	0.006	0.009	0.014	250m
	GW 8	0.014	0.014	0.014	0.014	1000m

The posterior 75th and 25th parameter quantiles for each calibrated soil, vegetation, and channel (Table S2), and median parameter values (Fig. S3) show the distribution of calibrated parameters for each model resolution.

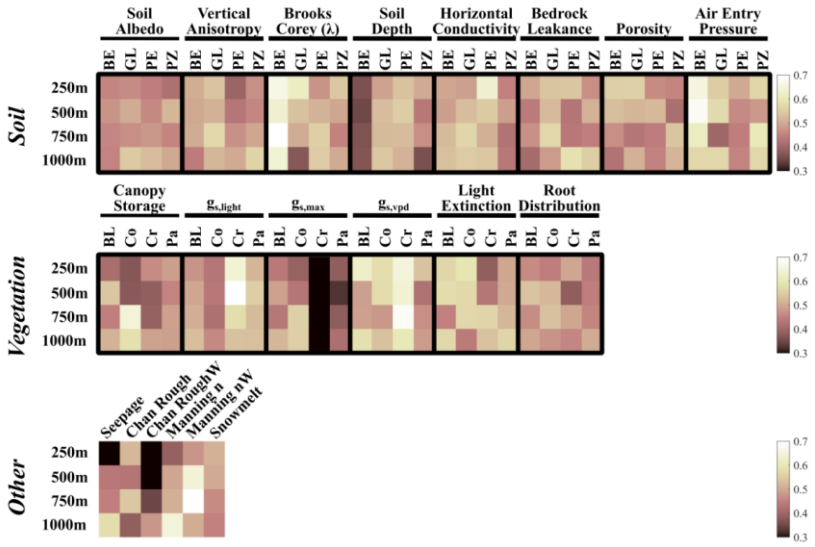

Figure S3: Median parameter value standardized from the maximum parameter range for all calibrated parameters in the soil, vegetation, and non-soil or vegetation dependent parameters. Soil types are classified as brown earth (BE), gley (GL), peat (PE), and podzols (PZ).

Fig. S3 shows the median calibrated parameter value, normalized on a scale between 0 (lowest value of parameter range) and 1 (highest value of parameter range). Darker colours indicate a skew of the calibrated parameters towards lower parameter values and lighter colours indicate a skew of calibrated parameters towards higher parameter values. The scales showed relatively limited differences for most parameters. Some parameter distributions shifts were similar across all model resolution, notably shallower soil depth and higher Brook-Corey lambda in brown earth (Fig. S3). The most sensitive parameters (e.g. anisotropy, conductivity, Manning's n, leakance, seepage) showed relatively smooth changes with model resolution. Particularly with finer resolutions, anisotropy (higher in BE and lower in PE and PZ), hydraulic conductivity (lower in BE, GL, PE), manning's n (lower), and seepage of groundwater into the channels (decreasing).

Table S2: The 75th and 25th percentiles of posterior parameter ranges for soil parameters (brown earth, gley, peat, and podzol, BE, GL, PE, and PZ, respectively), vegetation parameters (croplands, broadleaf, conifers, and pasturelands, Cr, BL, Co, and Pa, respectively), and channel parameters for each model scale (250, 500, 750, and 1000m). Percentages in parentheses indicate the percent change of the interquartile range from the a priori parameter range.

Soil					
		250m	**500m**	**750m**	**1000m**
Soil Albedo	BE	0.18 - 0.12 (18 %)	0.17 - 0.13 (-22 %)	0.18 - 0.13 (0 %)	0.18 - 0.13 (0 %)
	GL	0.18 - 0.12 (18 %)	0.17 - 0.13 (-22 %)	0.17 - 0.12 (0 %)	0.17 - 0.12 (0 %)
	PE	0.18 - 0.13 (0 %)	0.18 - 0.13 (0 %)	0.17 - 0.13 (-22 %)	0.17 - 0.12 (0 %)
	PZ	0.18 - 0.13 (0 %)	0.17 - 0.13 (-22 %)	0.18 - 0.13 (0 %)	0.17 - 0.13 (-22 %)
Vertical Aniso.	BE	0.31 - 0.13 (-5 %)	0.28 - 0.12 (-17 %)	0.30 - 0.10 (5 %)	0.29 - 0.09 (5 %)
	GL	0.31 - 0.10 (10 %)	0.33 - 0.11 (15 %)	0.30 - 0.08 (15 %)	0.29 - 0.10 (0 %)
	PE	0.32 - 0.13 (0 %)	0.32 - 0.14 (-5 %)	0.31 - 0.12 (0 %)	0.30 - 0.08 (15 %)
	PZ	0.30 - 0.11 (0 %)	0.30 - 0.12 (-5 %)	0.29 - 0.11 (-5 %)	0.30 - 0.11 (0 %)
Brooks Corey	BE	5.46 - 3.16 (2 %)	5.15 - 3.26 (-17 %)	5.00 - 3.13 (-18 %)	5.51 - 3.20 (3 %)
	GL	5.48 - 3.54 (-15 %)	5.68 - 3.69 (-12 %)	6.13 - 3.82 (3 %)	6.26 - 4.02 (0 %)
	PE	12.47 - 5.53 (7 %)	11.68 - 5.21 (0 %)	12.4 - 4.82 (15 %)	11.74 - 5.04 (3 %)
	PZ	5.31 - 3.35 (-4 %)	5.28 - 3.65 (-23 %)	5.61 - 3.37 (9 %)	5.51 - 3.40 (3 %)
Soil Depth	BE	7.67 - 4.09 (-17 %)	7.5 - 4.27 (-27 %)	7.58 - 3.84 (-13 %)	7.67 - 3.71 (-7 %)
	GL	7.27 - 2.17 (18 %)	6.65 - 2.7 (-7 %)	7.02 - 2.10 (15 %)	7.12 - 2.40 (10 %)
	PE	6.65 - 2.84 (-11 %)	6.99 - 2.49 (6 %)	6.60 - 2.32 (1 %)	7.02 - 2.47 (7 %)
	PZ	6.77 - 2.58 (-1 %)	7.75 - 2.94 (12 %)	7.55 - 2.84 (10 %)	7.35 - 3.22 (-3 %)
Horiz. Cond.	BE	$1.92x10^{-3}$ - $1.30x10^{-4}$ (-72 %)	$1.59x10^{-3}$ - $4.00x10^{-5}$ (-46 %)	$2.11x10^{-3}$ - $1.00x10^{-5}$ (-10 %)	$1.25x10^{-3}$ - $1.00x10^{-5}$ (-10 %)
	GL	$6.24x10^{-3}$ - $2.00x10^{-5}$ (0 %)	$4.41x10^{-3}$ – $1.00x10^{-5}$ (-1 %)	$3.58x10^{-3}$ - $1.00x10^{-5}$ (1 %)	$4.00x10^{-3}$ - $1.00x10^{-5}$ (1 %)
	PE	$1.55x10^{-3}$ - $1.00x10^{-5}$ (-13 %)	$3.82x10^{-3}$- $1.00x10^{-5}$ (1 %)	$2.78x10^{-3}$ - $3.00x10^{-5}$ (-20 %)	$4.88x10^{-3}$ - $1.00x10^{-5}$ (-20 %)
	PZ	$5.77x10^{-3}$ - $2.00x10^{-5}$ (0 %)	$8.06x10^{-3}$ - $1.00x10^{-5}$ (13 %)	$6.88x10^{-3}$ - $2.00x10^{-5}$ (5 %)	$1.26x10^{-2}$ - $3.00x10^{-5}$ (5 %)
Leak	BE	$1.06x10^{-6}$ - $5.60x10^{-9}$ (-28 %)	$2.90x10^{-6}$ - $6.00x10^{-9}$ (-11%)	$3.34x10^{-6}$ - $2.40x10^{-9}$ (5 %)	$7.63x10^{-6}$ - $6.30x10^{-9}$ (5 %)
	GL	$5.71x10^{-6}$ - $2.60x10^{-9}$ (11 %)	$4.57x10^{-6}$ - $6.20x10^{-9}$ (-5 %)	$2.23x10^{-6}$ - $4.10x10^{-9}$ (-9 %)	$1.82x10^{-6}$ - $3.10x10^{-9}$ (-9 %)
	PE	$3.43x10^{-6}$ - $1.50x10^{-9}$ (12 %)	$6.46x10^{-6}$ - $2.90x10^{-9}$ (11 %)	$5.63x10^{-6}$ - $5.30x10^{-9}$ (1 %)	$2.75x10^{-6}$ - $3.30x10^{-9}$ (1 %)
	PZ	$6.25x10^{-6}$ - $6.30x10^{-9}$ (0 %)	$2.55x10^{-6}$ - $6.40x10^{-9}$ (-14%)	$4.95x10^{-6}$ - $3.40x10^{-9}$ (5 %)	$5.55\ x10^{-7}$ - $4.60x10^{-9}$ (5 %)

Porosity	BE	0.48 - 0.37 (10 %)	0.46 - 0.38 (-22 %)	0.48 - 0.38 (0 %)	0.50 - 0.41 (-11 %)
	GL	0.47 - 0.35 (18 %)	0.47 - 0.37 (0 %)	0.48 - 0.40 (-22 %)	0.46 - 0.36 (0 %)
	PE	0.60 - 0.45 (-24 %)	0.63 - 0.43 (5 %)	0.63 - 0.43 (5 %)	0.61 - 0.41 (5 %)
	PZ	0.48 - 0.36 (29 %)	0.46 - 0.38 (-12 %)	0.46 - 0.37 (0 %)	0.46 - 0.37 (0 %)
Entry Pressure	BE	0.32 - 0.14 (-36 %)	0.33 - 0.12 (-21 %)	0.35 - 0.14 (-21 %)	0.40 - 0.15 (-4 %)
	GL	0.33 - 0.13 (-5 %)	0.34 - 0.14 (-5 %)	0.39 - 0.20 (-10 %)	0.32 - 0.17 (-33 %)
	PE	0.89 - 0.30 (3 %)	0.95 - 0.34 (7 %)	0.89 - 0.41 (-17 %)	0.92 - 0.32 (5 %)
	PZ	0.29 - 0.11 (18 %)	0.30 - 0.15 (0 %)	0.26 - 0.10 (6 %)	0.28 - 0.1 (18 %)
Seep.	All	1.72 - 0.17 (-85 %)	0.58 - 0.02 (-53 %)	0.50 - 0.02 (-49 %)	0.18 – 0.01 (-41 %)
Snow melt Coeff.	All	$1.5x10^{-7}$ – $6.0x10^{-8}$ (-46 %)	$1.7x10^{-7}$ - $6.0x10^{-8}$ (-44 %)	$1.6x10^{-7}$ - $6.0x10^{-8}$ (-41 %)	$1.6x10^{-7}$ - $7.0x10^{-8}$ (-62 %)
Vegetation					
		250m	**500m**	**750m**	**1000m**
Canopy Storage	Cr	$2.8x10^{-4}$ - $1.5x10^{-4}$ (-98 %)	$3.1x10^{-4}$ - $1.5x10^{-4}$ (-87 %)	$2.9x10^{-4}$ - 1.7 $x10^{-4}$ (-114 %)	$2.9x10^{-4}$ - $1.5x10^{-4}$ (-97 %)
	BL	$2.8x10^{-3}$ - $5.8x10^{-4}$ (-8 %)	$2.3x10^{-3}$ - $4.6x10^{-4}$ (-4 %)	3.2 $x10^{-3}$ - $5.8x10^{-4}$ (1 %)	$2.3x10^{-3}$ - $4.1x10^{-4}$ (2 %)
	Co	$3.3x10^{-3}$ - $6.1x10^{-4}$ (-1 %)	$3.8x10^{-3}$ - $5.2x10^{-4}$ (15 %)	$2.0x10^{-3}$ – $3.5x10^{-4}$ (2 %)	$2.1x10^{-3}$ - $3.6x10^{-4}$ (5 %)
	Pa	$2.9x10^{-4}$ - $1.5x10^{-4}$ (-90 %)	$3.0x10^{-4}$ - $1.4x10^{-4}$ (-86 %)	$3.1x10^{-4}$ - $1.4x10^{-4}$ (-80 %)	$3.0x10^{-4}$ - $1.4x10^{-4}$ (-81 %)
$g_{s,light}$	Cr	310 - 83 (-9 %)	299 - 45 (2 %)	341 - 86 (2 %)	361 - 98 (5 %)
	BL	399 - 132 (6 %)	359 - 135 (-11 %)	358 - 129 (-9 %)	366 - 126 (-4 %)
	Co	405 - 146 (4 %)	370 - 129 (-4 %)	388 - 153 (-6 %)	384 - 128 (3 %)
	Pa	345 - 132 (-16 %)	365 - 144 (-12 %)	339 - 70 (7 %)	322 - 65 (3 %)
gs,max	Cr	$2.32x10^{-2}$ - $1.28x10^{-2}$ (-97 %)	$2.23x10^{-2}$ - $1.11x10^{-2}$ (-81 %)	$2.27x10^{-2}$ - $1.05x10^{-2}$ (-75 %)	$2.34x10^{-2}$ - $1.30x10^{-2}$ (-97 %)
	BL	$6.40x10^{-3}$ - $2.10x10^{-3}$ (-4 %)	6.55 $x10^{-3}$ - 1.96 $x10^{-3}$ (5 %)	5.63 $x10^{-3}$ - $2.04x10^{-3}$ (-13%)	$5.97x10^{-3}$ - $2.04x10^{-3}$ (-7 %)
	Co	$7.10x10^{-3}$ - $2.00x10^{-3}$ (8 %)	6.28 $x10^{-3}$ - $1.91x10^{-3}$ (3 %)	$5.59x10^{-3}$ - $1.86x10^{-3}$ (-4 %)	$4.67x10^{-3}$ - $1.56x10^{-3}$ (-5 %)
	Pa	$6.00x10^{-3}$ - $1.6x10^{-3}$ (-14 %)	$7.80x10^{-3}$ - $1.31x10^{-3}$ (18 %)	$6.39x10^{-3}$ - $1.25x10^{-3}$ (8 %)	$6.68x10^{-3}$ - $1.23x10^{-3}$ (12 %)
gs,vpd	Cr	$1.5x10^{-4}$ - $1x10^{-5}$ (-34 %)	$1.5x10^{-4}$ – $1.0x10^{-5}$ (-33 %)	$9.0x10^{-5}$ - $1.0x10^{-6}$ (-42 %)	$1.8x10^{-4}$ - $1.0x10^{-5}$ (-34 %)
	BL	$4.0x10^{-4}$ - $1.0x10^{-5}$ (-11 %)	$1.9x10^{-3}$ - 0.00002 (4 %)	$1.0x10^{-3}$ - $1.0x10^{-5}$ (3 %)	$5.7x10^{-4}$ - $1x10^{-5}$ (-11 %)
	Co	$4.5x10^{-4}$ - $1.0x10^{-5}$ (-13 %)	$7.3x10^{-4}$ - $1.0x10^{-5}$ (-17 %)	$6.6x10^{-4}$ -1.0 $x10^{-5}$ (2 %)	$5.0x10^{-4}$ - $1x10^{-5}$ (-27 %)
	Pa	$3.7x10^{-4}$ - $1.0x10^{-5}$ (-33 %)	$1.4x10^{-3}$ - $2.0x10^{-5}$ (-9 %)	$5.5x10^{-4}$ – $1.0x10^{-5}$ (-13 %)	1.4 $x10^{-3}$ – $1.0x10^{-5}$ (6 %)
Light Extinction	Cr	0.64 - 0.50 (-7 %)	0.63 - 0.50 (-14 %)	0.61 - 0.49 (-22 %)	0.62 - 0.47 (0 %)
	BL	0.62 - 0.46 (6 %)	0.60 - 0.46 (-7 %)	0.61 - 0.48 (-14 %)	0.62 - 0.46 (6 %)
	Co	0.61 - 0.46 (0 %)	0.62 - 0.48 (-7 %)	0.62 - 0.48 (-7 %)	0.64 - 0.49 (0 %)
	Pa	0.61 - 0.49 (-22 %)	0.63 - 0.50 (-14 %)	0.63 - 0.47 (6 %)	0.60 - 0.47 (-14 %)
Root Distribution	Cr	7.60 - 3.50 (-18 %)	7.91 - 4.01 (-24 %)	6.94 - 3.38 (-33 %)	7.75 - 3.60 (-18 %)
	BL	3.70 - 1.40 (-5 %)	3.59 - 1.29 (-6 %)	3.78 - 1.25 (3 %)	3.69 - 1.77 (-24 %)
	Co	4.00 - 1.50 (4 %)	3.85 - 1.43 (-1 %)	3.49 - 1.26 (-9 %)	4.02 - 1.39 (7 %)
	Pa	7.70 - 2.80 (-1 %)	7.42 - 3.26 (-17 %)	7.83 - 3.61 (-16 %)	7.30 - 2.80 (-10 %)
Channel Parameters					
		250m	**500m**	**750m**	**1000m**

Chan Rough	24.72 - 15.46 (-8 %)	26.47 - 15.2 (12 %)	25.31 - 15.56 (-3 %)	26.86 - 15.78 (10 %)
Chan Rough(W)	13.74 - 10.07 (-31 %)	14.07 - 10.47 (-33 %)	13.41 - 9.31 (-20 %)	12.56 - 7.75 (-4 %)
Manning n	0.03 - 0.02 (0 %)	0.03 - 0.02 (0 %)	0.03 - 0.02 (0 %)	0.03 - 0.01 (67 %)
Manning n (W)	0.39 - 0.18 (-17 %)	0.37 - 0.04 (28 %)	0.26 - 0.06 (-22 %)	0.40 - 0.04 (36 %)

Model validation was conducted for the average flow years observed from 2015 – 2017. The data available for validation were not as robust as the calibration period because isotopic measurement didn't begin until 2018. Due to the severe drought in the catchment during 2018 (Smith et al., 2020;Kleine et al., 2020), stream, soil, and groundwater isotopes were not representative for validation, and 2019 isotopic data were required for calibration (calibration during a non-extreme drought). The trend of increasing efficiency with coarser model resolutions during validation are similar to the calibration (Table 4). Similarly, soil moisture, which showed higher efficiency for finer resolutions, showed higher efficiency for finer resolutions during validation. Discharge efficiency during validation was somewhat anomalous, with a lower efficiency at 250m than at coarser scales, contrary to the higher efficiency at finer resolutions in calibration.

Table S3: Median efficiency for the validation period 2015 – 2017 for discharge, evapotranspiration, latent heat, and soil moisture

		250m	500m	750m	1000m
Discharge	**Demnitz Mill**	0.35	0.36	0.43	0.44
Evapo-transpiration	**Forest**	0.52	0.48	0.60	0.61
	Alt Madlitz	0.47	0.45	0.49	0.53
	Conifer	0.02	0.25	0.33	0.23
Latent Heat	**Forest**	0.29	0.37	0.51	0.50
	Alt Madlitz	0.23	0.28	0.33	0.34
	Conifer	0.05	0.28	0.37	0.28
Soil Moisture	**Forest**	0.16	-0.29	0.03	0.15
	Alt Madlitz	0.41	0.11	-0.16	-0.04

Supplementary Material 3: Temporal changes in water age estimations

All model resolutions showed a similar seasonal trend of water ages in layer 1 (Table S4), varying between the oldest water in spring and the youngest water in the summer. The temporal variation changes consistently across the catchment, with the spatial variability of water ages shown on Fig. 7. Temporal trends of water ages in layer 2 were slightly different from layer 1 (Table S4) and revealed subtle but trivial differences between model resolutions. The oldest water was estimated in autumn and the youngest water in the winter, a direct seasonal shift from layer 1.

Table S4: Estimated seasonal water ages in soil layers 1 and 2, transpiration, and groundwater residence time for each model scale. Seasons are defined as winter (Dec – Feb), spring (Mar-May), summer (Jun – Aug), and autumn (Sep – Nov).

		Scale			
	Season	**250m**	**500m**	**750m**	**1000m**
Layer 1 Age (days)	**Winter**	73 ± 16	58 ± 13	59 ± 12	62 ± 13
	Spring	93 ± 22	70 ± 18	72 ± 16	77 ± 17
	Summer	47 ± 14	29 ± 8	28 ± 8	28 ± 9
	Autumn	48 ± 12	35 ± 6	34 ± 6	33 ± 7
Layer 2 Age (days)	**Winter**	212 ± 192	159 ± 131	144 ± 112	165 ± 87
	Spring	219 ± 196	184 ± 143	175 ± 125	196 ± 87
	Summer	233 ± 196	181 ± 138	139 ± 126	190 ± 89
	Autumn	245 ± 191	178 ± 127	163 ± 115	186 ± 88
Transpiration Age (days)	**Winter**	147 ± 153	156 ± 158	180 ± 187	202 ± 213
	Spring	276 ± 236	296 ± 258	332 ± 280	357 ± 310
	Summer	335 ± 281	388 ± 357	453 ± 396	455 ± 397
	Autumn	305 ± 270	339 ± 351	390 ± 388	426 ± 374
Groundwater Mean Residence Time (years)	**Winter**	13.3 ± 8.0	21.4 ± 18.9	19.3 ± 18.4	23.5 ± 34.8
	Spring	13.3 ± 8.5	21.8 ± 19.6	18.4 ± 18.5	22.4 ± 33.4
	Summer	14.4 ± 8.7	23.3 ± 19.4	20.6 ± 18.9	24.2 ± 35.3
	Autumn	16.2 ± 9.6	27.2 ± 20.5	24.8 ± 20.3	26.4 ± 36.8

Supplementary Material 4: Calibrated rooting distribution

The rooting distributions in EcH$_2$O(-iso) are defined using the depth of each soil layer and an exponential function (Kuppel et al., 2018) (single shape parameter, Root Distribution, Table S2). Lower values of the exponential parameter distribute roots more equally through all soil layers, while high values distribute more roots to near-surface soil layers. Croplands and pasturelands were estimated to have a higher proportion of roots in the near-surface soils for all model resolution (Fig. S4), despite a larger a priori root distribution range than conifers and broadleafs (Table S2). For the broadleaf and conifer forests, optimization of the root distribution showed a more uniform distribution of roots with depth (note that layer 1 and 2 are much smaller volumes than layer 3).

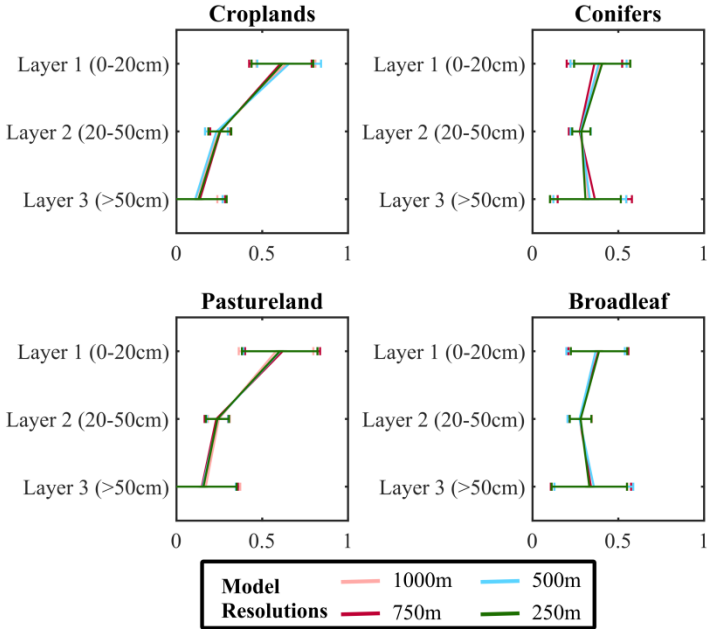

Figure S4: Estimated rooting profiles from the calibrated rooting distribution parameter.

Supplementary Material 5: Correlation matrix of storage-flux-age-vegetation-soil

The correlation of primary fluxes; evapotranspiration (ET), soil evaporation (Es), transpiration (Tr), and groundwater recharge (Re), primary storage; layer 1 (L1), layer 2 (L2), layer 3 (L3), and groundwater (GW), and primary storage and flux ages; layer 1 (L1), layer 2 (L2), layer 3 (L3), and transpiration (Tr), is essential to understand how the catchment response may change under varying conditions. Additionally, how the primary drivers of the fluxes, storage and water ages, vegetation and soils are correlated across the catchment provides useful information for how management decisions may affect the catchment hydrology and ecological growth. The annual sum of fluxes, annual average storage and water ages, proportion of vegetation (cropland = Cr, broadleaf = BL, conifer = Co, and pastureland = Pa), and soil (brown earth = BE, gley = GL, Peat = PE, and podzol = PZ) were spatially correlated with the Spearman rank correlation. The Spearman rank correlation was used as it does not assume a normal distribution. The significance of the correlations was determined by the 95th percentile for all spatial locations up to the extent of the Demnitz Mill discharge location (Fig. 1a). Modelled fluxes, storages, and ages outside this spatial domain were not considered. The colour-coded correlation matrix (Fig. S5) shows the correlation for each age, storage, flux, vegetation, and soil relationship for each model resolution. Deep blue colours indicate a strong positive correlation (e.g. storage in layers 1 and 2 to soil evaporation) while deep red values indicate a strong negative correlation (e.g. all ages correlated to groundwater recharge). White squares indicate that no significant spatial correlation was found.

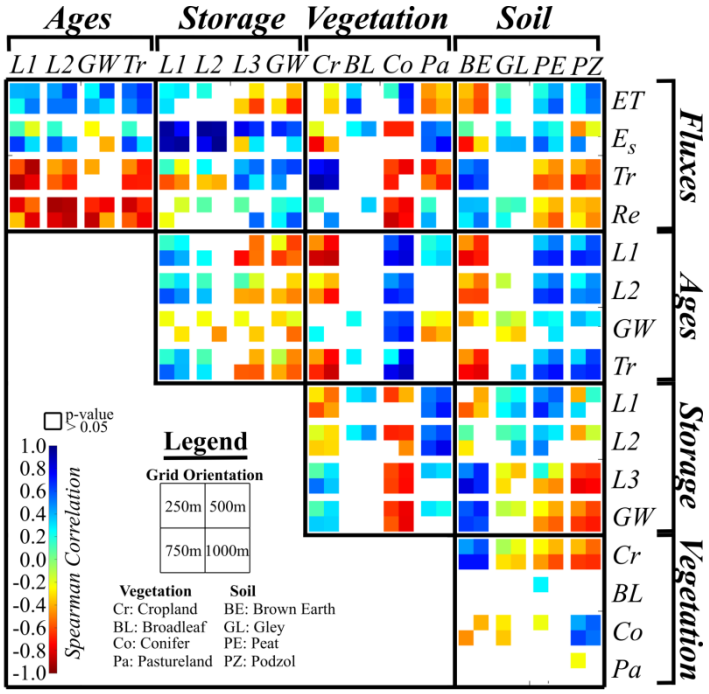

Figure S5: Spearman rank correlation matrix of flux-age-storage-vegetation-soil with annual average values (flux, and, and storage). No colours indicate that the correlations are insignificant to 95% threshold.

Supplementary Material 6: Time series of evapotranspiration components for different vegetation

The evapotranspiration components, transpiration, soil evaporation, and interception evaporation, are highly temporally dynamic, changing with the season and interannually. Due to relatively dry periods during the study period (2018 – 2019), the long term average of the components may be artificially skewed. Figure S6 shows the monthly average proportion of transpiration, soil evaporation, and interception evaporation from evapotranspiration, with median (solid line) and upper and lower simulation bounds (shaded area) for each model resolution and primary vegetation type. Note the scale of time-series for peak values (peak soil evaporation and interception evaporation during the winter, not the summer).

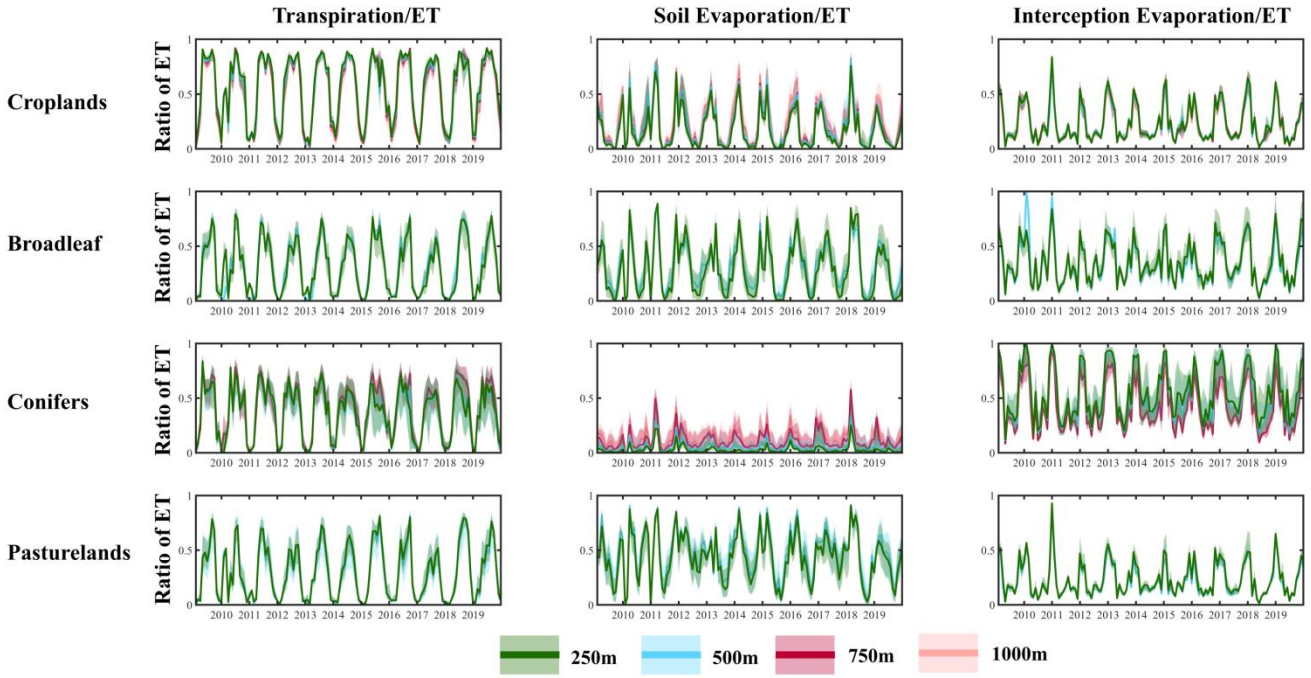

References

Ala-aho, P., Tetzlaff, D., McNamara, J. P., Laudon, H., and Soulsby, C.: Using isotopes to constrain water flux and age estimates in snow-influenced catchments using the STARR (Spatially distributed Tracer-Aided Rainfall–Runoff) model, Hydrology and Earth System Sciences, 21, 5089-5110, 10.5194/hess-21-5089-2017, 2017.

Boyle, D. P., Gupta, H. V., and Sorooshian, S.: Toward improved calibration of hydrologic models: Combining the strengths of manual and automatic methods, Water Resources Research, 36, 3663-3674, 10.1029/2000wr900207, 2000.

Douinot, A., Tetzlaff, D., Maneta, M., Kuppel, S., Schulte-Bisping, H., and Soulsby, C.: Ecohydrological modelling with EcH2O-iso to quantify forest and grassland effects on water partitioning and flux ages, Hydrological Processes, 10.1002/hyp.13480, 2019.

Kleine, L., Tetzlaff, D., Smith, A., Wang, H., and Soulsby, C.: Using isotopes to understand evaporation, moisture stress and re-wetting in catchment forest and grassland soils of the summer drought of 2018, Hydrol. Earth Syst. Sci. Discuss., 2020, 1-29, 10.5194/hess-2020-81, 2020.

Kuppel, S., Tetzlaff, D., Maneta, M. P., and Soulsby, C.: EcH2O-iso 1.0: water isotopes and age tracking in a process-based, distributed ecohydrological model, Geoscientific Model Development, 11, 3045-3069, 10.5194/gmd-11-3045-2018, 2018.

Smith, A., Tetzlaff, D., Kleine, L., Maneta, M. P., and Soulsby, C.: Isotope-aided modelling of ecohydrologic fluxes and water ages under mixed land use in Central Europe: The 2018 drought and its recovery, Hydrological Processes, 34, 3406-3425, 10.1002/hyp.13838, 2020.